RSC Advances

This is an *Accepted Manuscript*, which has been through the Royal Society of Chemistry peer review process and has been accepted for publication.

Accepted Manuscripts are published online shortly after acceptance, before technical editing, formatting and proof reading. Using this free service, authors can make their results available to the community, in citable form, before we publish the edited article. This *Accepted Manuscript* will be replaced by the edited, formatted and paginated article as soon as this is available.

You can find more information about *Accepted Manuscripts* in the Information for Authors.

Please note that technical editing may introduce minor changes to the text and/or graphics, which may alter content. The journal's standard Terms & Conditions and the Ethical guidelines still apply. In no event shall the Royal Society of Chemistry be held responsible for any errors or omissions in this *Accepted Manuscript* or any consequences arising from the use of any information it contains.

ROYAL SOCIETY OF CHEMISTRY

www.rsc.org/advances

CREATED USING THE RSC ARTICLE TEMPLATE (VER. 3.1) - SEE WWW.RSC.ORG/ELECTRONICFILES FOR DETAILS

ARTICLE TYPE www.rsc.org/xxxxxx | XXXXXXXX

Functional Groups on POSS Nanoparticles Influence the Self-Assembled Structures of Diblock Copolymer Composites

Yi-Syuan Lu and Shiao-Wei Kuo*

Received (in XXX, XXX) Xth XXXXXXXXX 200X, Accepted Xth XXXXXXXXX 200X
First published on the web Xth XXXXXXXXX 200X
DOI: 10.1039/b000000x

We investigated the influence of the functional groups presented by polyhedral oligomeric silsesquioxane (POSS) nanoparticles (NPs) on the self-assembled structures formed by diblock copolymer composites. We blended two amorphous POSS derivatives, octakis[dimethyl(4-phenethyl)siloxy]silsesquioxane (OS-POSS) and octakis[dimethyl(4-hydroxyphenethyl)siloxy]silsesquioxane (OP-POSS), with the block copolymer poly(styrene-*b*-4-vinyl pyridine) (PS-*b*-P4VP). This long-range order transformed into distorted lamellar structures when we blended PS-*b*-P4VP with the OS-POSS NPs due to the relatively weak intermolecular hydrophobic forces between the aromatic groups of OS-POSS and the PS block segments. In contrast, we obtained well-defined self-assembled structures, in the form of block copolymer nanocomposites, after blending PS-*b*-P4VP with the OP-POSS NPs; an order–order morphological transition occurred upon increasing the content of OP-POSS NPs in the PS-*b*-P4VP diblock copolymer. Transmission electron microscopy and small-angle X-ray scattering revealed morphologies exhibiting high degrees of long-range order, namely lamellar structures at low OP-POSS NP contents, hexagonally packed cylindrical structures at higher OP-POSS NP contents, and a body-centered cubic spherical structure at the highest OP-POSS NP content, due to relatively strong hydrogen bonding interactions between the OH groups of the OP-POSS NPs and the pyridyl groups of the P4VP block segments.

Introduction

Self-assembled macromolecules, such as block copolymer/nanoparticle (BCP/NP) composites, have potential applications in sensors, photonics, and nanodevices. Neat block copolymers can self-assemble to form periodic nanostructures, including spheres, cylinders, lamellae, and bicontinuous gyroids, with characteristic length scales in the range from 10 to 100 nm.[1,2] The type of structure is strongly dependent on the overall number-average degree of polymerization, the volume fractions of the components of the BCP, and the Flory–Huggins segment–segment interaction parameter. The dispersion of NPs in a BCP is associated with a change in enthalpy arising from the creation of polymer–NP interfaces; a decrease in polymer conformational entropy can be accommodated in the presence of a limited number of such NPs.[3–6]

In general, the use of ligands that are compatible with only one of the blocks can lead to preferential segregation of the NPs within the compatible domain. For example, Kramer et al. controlled the distribution of NPs in microphase-separated structures of poly(styrene-*b*-2-vinyl pyridine) (PS-*b*-P2VP) BCPs by using PS or P2VP homopolymers as ligands for the NPs.[7–11] In such a system in which the ligand is chemical identical to one of the blocks, the addition of each enthalpically neutral particle carries an entropic penalty that pushes the system close to disorder at higher volume fractions of the NPs; this phenomenon is similar to that in BCP/homopolymer blend systems lacking strong intermolecular interactions.[12,13] Recently, strong hydrogen bonding has been exploited to blend BCPs with homopolymers, significantly enhancing the miscibility and swelling of the BCP domain without macrophase separation or corresponding order–order morphological transitions,[14–24] similar to the phenomena encountered in BCP/NP systems.[25–36] For example, CdS, CdSe, Au, and silicone (Si) NPs modified on their surfaces with OH functional groups can be positioned within the poly(ethylene oxide) (PEO) or poly(4-vinylpyridine) (P4VP) domains of diblock copolymers. The NP-induced transformations of diblock copolymers have been investigated in several previous studies,[25–36] essentially all of which involved systems where the NPs were immiscible with block A but interacted favorably with block B. Because of the presence of intermolecular hydrogen bonding, the macrophase separation of the NPs could be suppressed significantly in favor of microphase separation. Our motivation for this study was to understand the different effects of the ligands of NPs when either chemically identical to one of the blocks (i.e., PS) or having the ability to hydrogen bond to one of the blocks (i.e., P4VP). Both systems may allow us to make general predictions regarding the structures of NPs in BCPs to realize their potential applications as multifunctional organic/inorganic hybrid materials.

In this study, we report a new system comprising the diblock copolymer PS-*b*-P4VP, prepared through nitroxide-mediated radical polymerization, and polyhedral oligomeric silsesquioxane (POSS) cages as the NPs. POSS compounds, which are unique cage-like structures possessing nanoscale dimensions in the range 1–3 nm, are particularly interesting components for the preparation of hybrid materials.[37–39] The dimensions of POSS NPs are generally much smaller than the radii of gyration of typical polymers and may be viewed as both solvent molecules and NPs. These inorganic/organic hybrid architectures contain an inner inorganic framework composed of silicon and oxygen atoms [$(SiO_{1.5})_x$] surrounded by organic substituents.[40–44] Through hydrosilylations of unsaturated monomers with octakis(dimethylsiloxy)silsesquioxane $Q_8M_8^H$, mediated by Karstedt's catalyst (a platinum divinylsiloxane complex), we can obtain various POSS derivatives possessing distinct functionalities. In previous studies of POSS-based nanocomposites,[45–48] we synthesized and characterized the two amorphous POSS derivatives (Scheme 1) octakis[dimethyl(4-phenethyl)siloxy] silsesquioxane (OS-POSS) and

Department of Materials and Optoelectronic Science, National Sun Yat-Sen University, Kaohsiung, 804, Taiwan.
E-mail: kuosw@faculty.nsysu.edu.tw

RSC Advances Accepted Manuscript

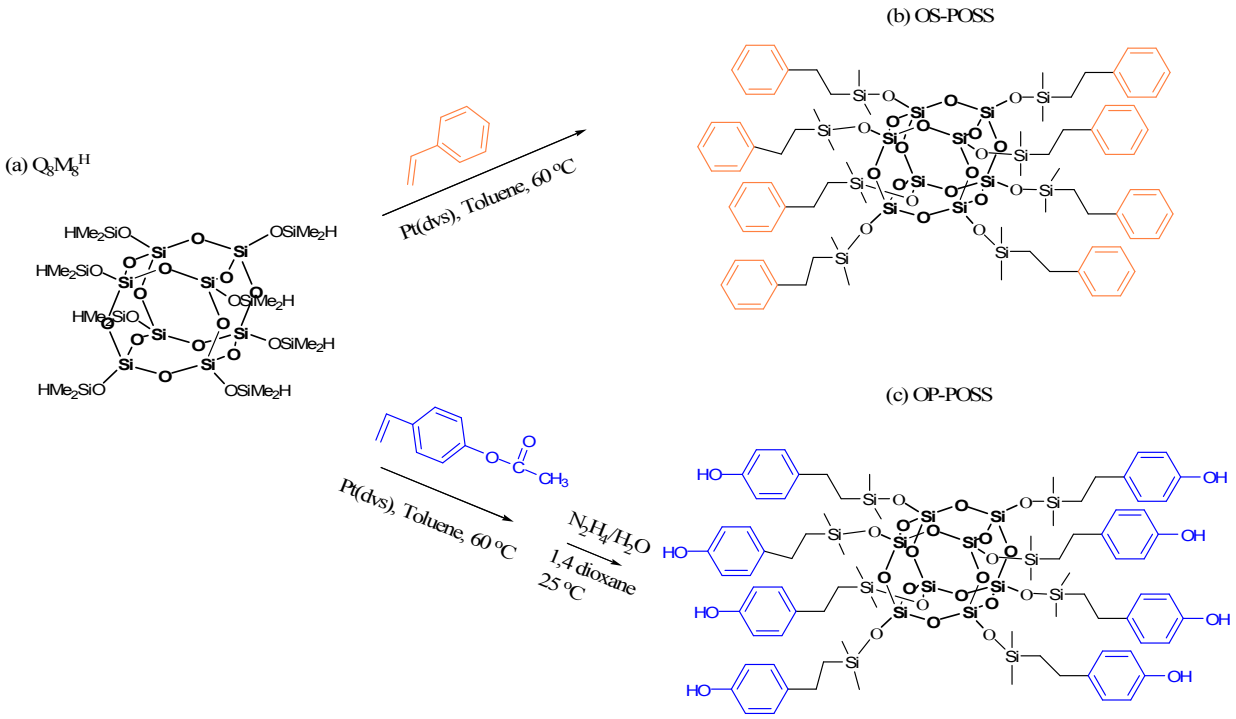

Scheme 1: Syntheses and chemical structures of (a) $Q_8M_8^H$, (b) OS-POSS, and (c) OP-POSS

octakis[dimethyl (4-hydroxyphenethyl)siloxy]silsesquioxane (OP-POSS). From their chemical structures, we anticipated that OS-POSS and OP-POSS would prefer to be located within the PS and P4VP domains, respectively, stabilized through intermolecular aromatic hydrophobic forces and hydrogen bonding interaction, respectively. We also expected the hydrogen bonding interactions between OP-POSS and P4VP to be stronger than the aromatic hydrophobic forces between OS-POSS and PS. We have used differential scanning calorimetry (DSC), transmission electron microscopy (TEM), small-angle X-ray scattering (SAXS), and Fourier transform infrared (FTIR) spectroscopy to characterize the self-assembly and specific interactions within these OS-POSS/PS-*b*-P4VP and OP-POSS/PS-*b*-P4VP hybrids.

Experimental Section

Materials

$Q_8M_8^H$ POSS was obtained from Hybrid Plastics. 4-Acetoxystyrene (96%), styrene, 4-vinylpyridine, hydrazine monohydrate (98%), platinum(0)/1,3-divinyl-1,1,3,3-tetramethyldisiloxane complex solution [Pt(dvs)] in xylene (Pt content: ca. 2%) were obtained from Aldrich Chemical (USA). The diblock copolymer poly(styrene-*b*-4-vinylpyridine) (PS_{216}-*b*-$P4VP_{257}$; M_n = 49,400 g/mol; PDI = 1.12) was synthesized through nitroxide-mediated radical polymerization. Octakis[dimethyl(phenethyl)siloxy] silsesquioxane (OS-POSS; M_n = 1850 g/mol) was prepared through hydrosilylation of styrene monomers with octakis(dimethylsiloxy)silsesquioxane ($Q_8M_8^H$).[45] Octakis[dimethyl(4-hydroxyphenethyl)siloxy]silsesquioxane (OP-POSS; M_n = 1978 g/mol) was synthesized through a simple two-step synthesis: hydrosilylation of 4-acetoxystyrene with $Q_8M_8^H$ and subsequent hydrolysis of the acetoxy units (Scheme 1).[45–48] Details of the synthesis and characterization of PS-*b*-P4VP, OS-POSS, and OP-POSS are available elsewhere.[45–49]

BCP/NP Blends

Blend samples containing various weight fractions of PS-*b*-P4VP with OS-POSS or OP-POSS were prepared through solution-casting. A DMF solution containing 5 wt% of the blend was stirred for 8–10 h and then cast on a Teflon dish. The solvent was evaporated slowly at 80 °C for 1 day and then the sample was dried in a vacuum oven at 200 °C.

Characterization

The thermal properties of the BCP/NP blend films were determined through DSC analysis using a TA Q-20 instrument; the scan rate was 20 °C/min within the temperature range 0–250 °C. The glass transition temperature (T_g) is defined herein as the midpoint of the heat capacity transition between the upper and lower points of deviation from the extrapolated liquid and glass lines. FTIR spectra of the polymer blend films were recorded using the conventional KBr disk method with a Bruker Tensor 27 FTIR spectrophotometer (32 scans; spectral resolution: 1 cm^{-1}); the films were sufficiently thin to obey the Beer–Lambert law. IR spectra recorded at elevated temperatures were obtained by using a cell mounted inside the temperature-controlled compartment of the spectrometer. The sample chamber was purged with N_2 during the measurement process to maintain dry sample films. SAXS data were collected using the BL17A1 wiggler beamline of the National Synchrotron Radiation Research Center (NSRRC), Taiwan. All temperature-resolved SAXS measurements were performed at several temperatures on a hot-stage under an atmosphere of dry N_2. The samples were sealed between two Kapton windows (thickness: 12 μm). An X-ray beam having a diameter of 0.5 mm and a wavelength (λ) of 1.1273 Å was used for the SAXS measurements (Q range: 0.015–0.3 $Å^{-1}$). TEM experiments were conducted using a JEOL 2100 microscope (Japan) operated at 200 kV. Ultrathin sections of the samples were prepared using a Leica Ultracut S microtome equipped with a diamond knife. Slices (thickness: ca. 700 Å) were cut at room temperature. The ultrathin sections of the thin films of the PS-*b*-

RSC Advances Accepted Manuscript

This journal is © The Royal Society of Chemistry [year]

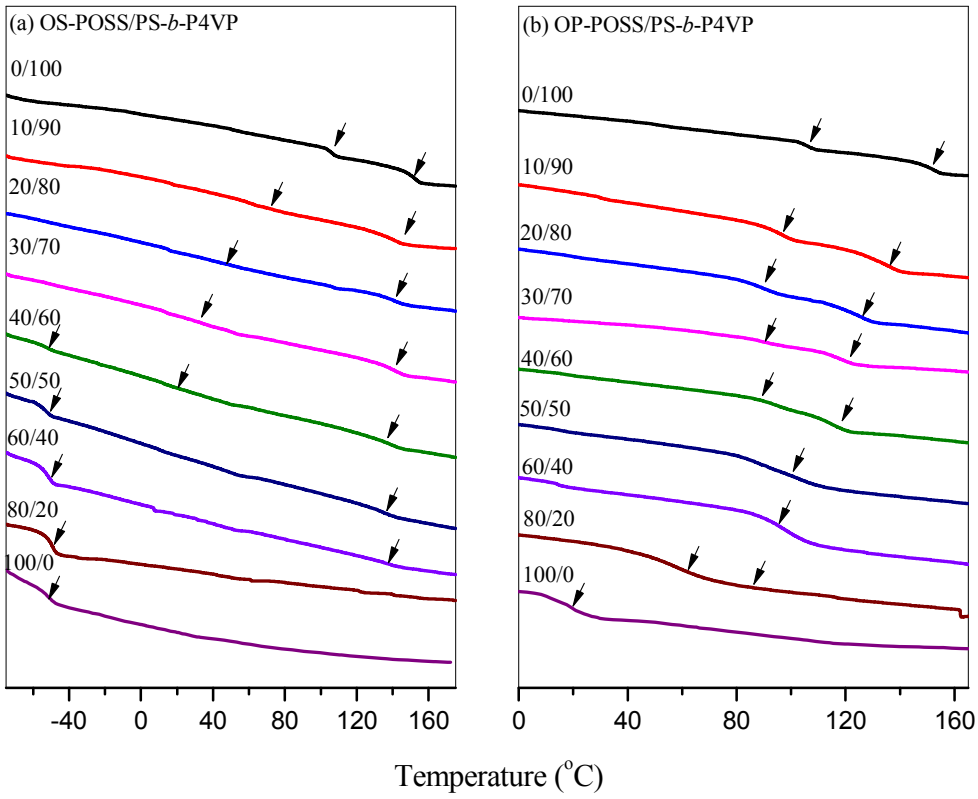

Figure 1: DSC thermograms of (a) OS-POSS/PS-*b*-P4VP and (b) OP-POSS/PS-*b*-P4VP NP hybrids.

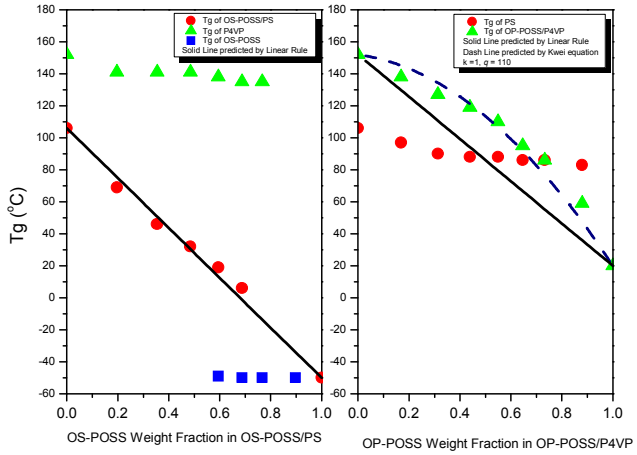

Figure 2: Glass transition behavior of (a) OS-POSS/PS-*b*-P4VP and (b) OP-POSS/PS-*b*-P4VP hybrids.

P4VP/OS-POSS (or OP-POSS) hybrids were placed onto Cu grids coated with C supporting films. TEM images of thin films of pure PS-*b*-P4VP and the PS-*b*-P4VP/OS-POSS hybrid were recorded using samples stained with I_2 to reveal the P4VP domains, but those of the PS-*b*-P4VP/OP-POSS hybrid were recorded without any staining.

Results and Discussion

Figure 1 displays conventional second-run DSC thermograms, obtained at a heating rate of 20 °C/min, of (a) OS-POSS/PS-*b*-P4VP and (b) OP-POSS/PS-*b*-P4VP hybrids of various compositions. The glass transition temperatures of the pure OS-POSS and OP-POSS NPs were –51 and +18 °C, respectively. These glass transition temperatures are significantly lower than those typically obtained for corresponding high-molecular-weight polymers [polystyrene: 100 °C; poly(vinyl phenol): 150–180 °C],[50] presumably because the degree of polymerization in these functional POSS derivatives was only 8.[45–48] The pure diblock copolymer PS-*b*-P4VP displayed two glass transition temperatures, reflecting the two different types of segments present in the polymer chain. Our DSC analysis revealed that the lower value of T_g of PS-*b*-P4VP occurred near 106 °C, indicating the presence of a large content of PS segments. We assign the higher value of T_g (ca. 152 °C) to the P4VP segments in the copolymer. Notably, the value of T_g of the PS block (106 °C) of PS-*b*-P4VP is higher than that of the PS homopolymer (ca. 100 °C at the same molecular weight), due to the hard confinement of the P4VP block (T_g = 152 °C). Table 1 summarizes the properties of these two POSS-related composites and the block copolymer PS-*b*-P4VP.

Figure 1(a) reveals that the value of T_g of the PS block decreased significantly, whereas that of the P4VP block remained almost unchanged (decreased only slightly), upon increasing the OS-POSS content at relatively low compositions (<40 wt%). This phenomenon is consistent with the OS-POSS NPs dissolving in the PS blocks, because the functional groups presented by the OS-POSS NPs were chemically identical to the PS blocks, allowing stabilization of the hybrids through intermolecular aromatic hydrophobic forces. Figure 2(a) summarizes the glass transition behavior of the OS-POSS/PS domains. Clearly, a linear

RSC Advances Accepted Manuscript

Table 1: Thermal properties of the OS-POSS, OP-POSS, and PS-*b*-P4VP samples used in this study.

Samples	Molar Mass	Glass Transition Temperature[c]
	M_n (g/mol)	(°C)
OS-POSS	1850[a]	–51
OP-POSS	1978[a]	18
PS-*b*-P4VP	49,400[b]	106/152

[a] Obtained from MALDI-TOF mass spectra
[b] Obtained from GPC and ^{1}H NMR spectra
[c] Obtained from the second run of DSC thermograms (heating rate: 20 °C/min)

rule can be predicted, indicating that the OS-POSS NPs and the PS polymer chains do not undergo any specific interactions, such as hydrogen bonding, but instead feature only weak intermolecular aromatic hydrophobic forces in their hybrid system. In addition, we also observed a glass transition for OS-POSS at a value of T_g of –51 °C at relatively high OS-POSS contents (>40 wt%), indicating that macrophase separation occurred; the addition of each enthalpically neutral OS-POSS NP carried an entropic penalty that pushed the system close to disorder at a higher volume fraction of the NPs, similar to the behavior of BCP/homopolymer blend systems that lack strong intermolecular interactions.[12,13,17]

In contrast, we suspected that added OP-POSS NPs would interact preferentially with the P4VP blocks through strong hydrogen bonding interactions of the OH groups of OP-POSS with the pyridyl groups of P4VP. At lower contents of OP-POSS NPs (<40 wt%), we observed two values of T_g; we assign the lower (ca. 92–106 °C) to a PS-dominant phase, which had phase-separated from the OP-POSS/P4VP hybrid complex, and the higher (ca. 116–152 °C) to the phase of a hydrogen-bonded OP-POSS/P4VP hybrid complex. The depression of the glass transition behavior in the PS domains was probably due to the lowering of the value of T_g of the OP-POSS/P4VP domains (i.e., more flexible chains) upon increasing the content of OP-POSS NPs. At a relatively high content of OP-POSS NPs (50 or 60 wt%), we detected only a single, but broad, endothermic event near 94–98 °C. Here, we suspect that the glass transition of the miscible OP-POSS/P4VP microphase had, by coincidence, dropped to the same temperature range as that of the PS segment, such that the two could not be resolved. A further increase in the content of OP-POSS NPs to 80 wt% caused the two glass transitions to reappear: the lower (ca. 60 °C) was due to the hydrogen-bonded OP-POSS/P4VP hybrid complex and the higher (ca. 90 °C) was due to the PS domains, as would be expected. Figure 2(b) summarizes the glass transition behavior of the OP-POSS/P4VP hybrid complexes. Interestingly, the values of T_g of the OP-POSS/P4VP hybrid complex domain exhibited a positive deviation from the linear rule. The Kwei equation[51] is usually employed to characterize systems displaying specific interactions:

$$T_g = \frac{W_1 T_{g1} + kW_2 T_{g2}}{W_1 + kW_2} + qW_1W_2 \qquad (1)$$

where W_1 and W_2 are the weight fractions of the components, T_{g1} and T_{g2} are the corresponding glass transition temperatures, and k and q are fitting constants. The parameter q represents the strength of the specific interactions in the system; it reflects a balance between the breaking of self-association interactions and the forming of inter-association interactions. From nonlinear least-squares best fits of the plots for the OP-POSS/P4VP complexes, we obtained values of k and q of 1 and 110, respectively. The positive value of q suggests that intermolecular

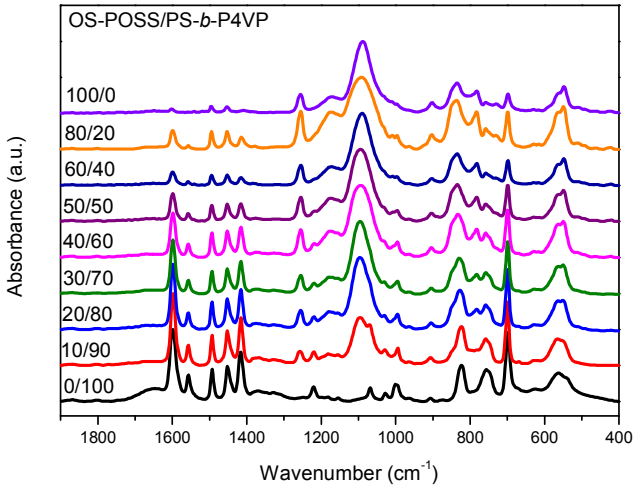

Figure 3: FTIR spectra, recorded at room temperature, of OS-POSS/PS-*b*-P4VP NP hybrids of various compositions.

hydrogen bonding in the OP-POSS/P4VP hybrid complex was stronger than the self-association hydrogen bonds of OP-POSS. In addition, no macrophase separation occurred when we blended the OP-POSS NPs in PS-*b*-P4VP (in contrast to the situation when adding the OS-POSS NPs), presumably because of the strong hydrogen bonding interactions between the OH group of OP-POSS and the pyridyl groups of P4VP.

Infrared spectroscopy is a highly effective method for investigating hydrogen bonding interactions in polymer complexes.[52] Figure 3 presents the FTIR spectra of OS-POSS/PS-*b*-P4VP blends at room temperature. The absence of any absorption shifts indicates that no strong specific interactions were present in this hybrid system. In contrast, the FTIR spectra in Figure 4 confirm the existence of hydrogen bonds between the PS-*b*-P4VP copolymer and the OP-POSS NPs. The spectrum of OP-POSS features two major unresolved bands in the OH stretching region: one corresponding to the free OH groups at 3525 cm^{-1} and another, broader band centered at 3340 cm^{-1} arising from the hydrogen-bonded OH groups (self-association). The intensity of the signal for the free OH groups decreased gradually upon increasing the content of the diblock copolymer PS-*b*-P4VP, as we had expected. This signal for the free OH groups disappeared essentially when the content of PS-*b*-P4VP reached 50 wt%, indicating that more of the OH groups formed hydrogen bonds with pyridyl groups when the concentration of the pyridyl groups increased. Meanwhile, the peak frequency of the broad band shifted to lower wavenumber upon increasing the PS-*b*-P4VP content, reflecting a distribution of hydrogen bonds (i.e., both OH···OH interactions among the OP units and OH···pyridyl interactions between the OP-POSS and P4VP units). This feature also revealed that the interaction between the OH group of OP-POSS and the pyridyl units of P4VP became the dominant one in blends that were rich in PS-*b*-P4VP. Therefore, we assign the band at 3150 cm^{-1} to the OH groups of OP-POSS that were hydrogen-bonded to the pyridyl units of the P4VP block. We used the difference in frequency ($\Delta\nu$) between the signals of the hydrogen-bonded and free OH groups to roughly estimate the average strength of hydrogen bonding.[52] In this respect, the hydrogen bonds formed between the OH groups of OP-POSS and the pyridyl units of P4VP in the diblock copolymer ($\Delta\nu$ = 375 cm^{-1}) were stronger than those between pairs of OP-POSS moieties ($\Delta\nu$ = 185 cm^{-1}).

In addition to OH stretching, some of the characteristic modes of the pyridyl rings were also sensitive to the presence of

RSC Advances Accepted Manuscript

This journal is © The Royal Society of Chemistry [year]

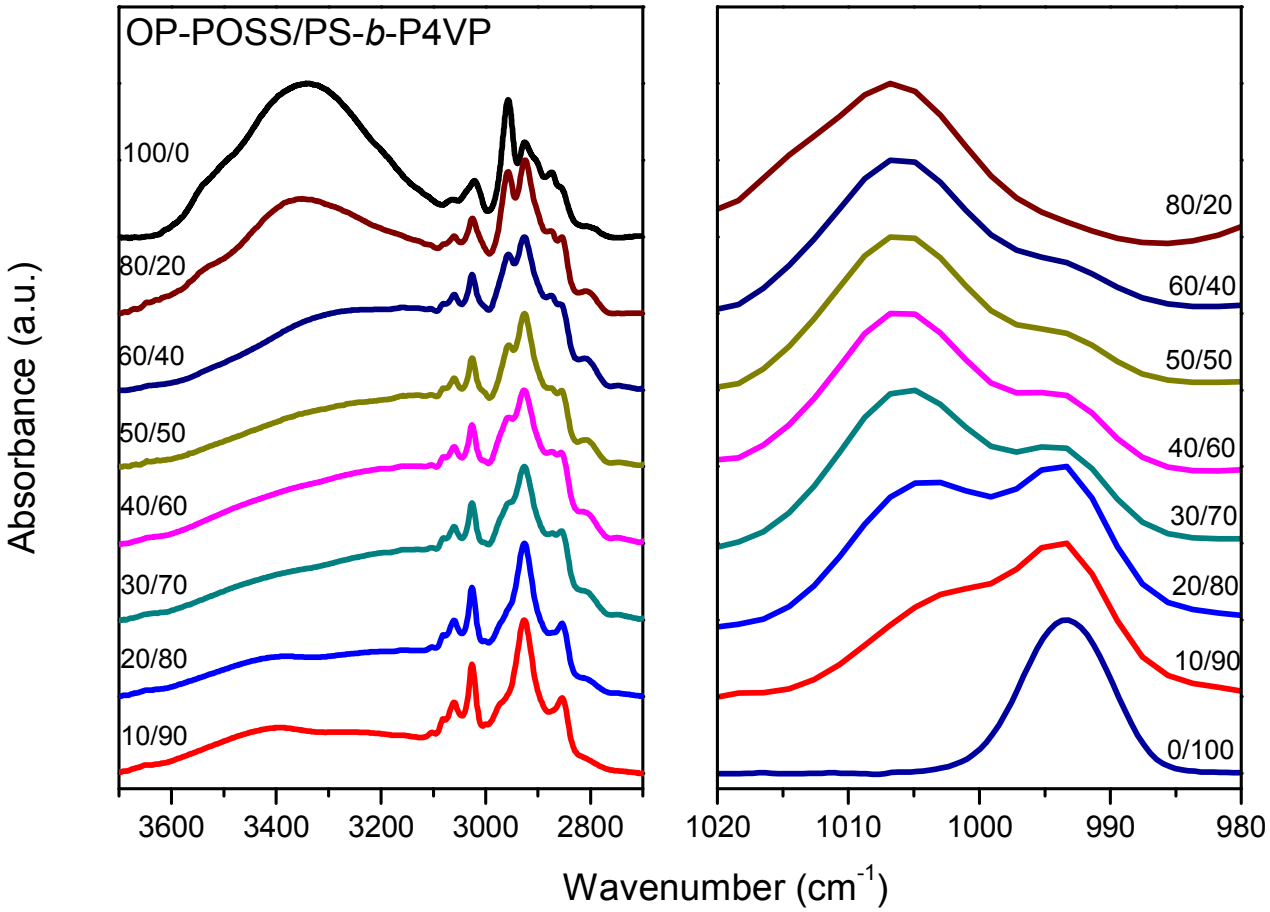

Figure 4: FTIR spectra, recorded at room temperature, of OP-POSS/PS-*b*-P4VP NP hybrids of various compositions: (a) OH and (b) pyridyl regions.

Table 2: Fractions of hydrogen bonded units in OP-POSS/PS-*b*-P4VP at room temperature

OP-POSS/ PS-*b*-P4VP	Free pyridyl rings			Hydrogen-bonded pyridyl rings			f_b (%)
	ν (cm^{-1})	$W_{1/2}$	A_f (%)	ν (cm^{-1})	$W_{1/2}$	A_b (%)	
0/100	993	10	100	–	–	–	–
10/90	993	10	51.4	1003	11	48.6	48.6
20/80	994	10	43.1	1004	11	56.9	56.9
30/70	994	10	36.8	1005	11	63.2	63.2
40/60	994	10	25.7	1005	11	74.3	74.3
50/50	994	9	20.1	1006	12	79.9	79.9
60/40	994	9	16.1	1006	12	83.9	83.9
80/20	993	9	4.2	1006	12	95.8	95.8

hydrogen bonds. We could use the band at 993 cm^{-1} to analyze the hydrogen bonding interactions between the OH group of OP-POSS and the pyridyl groups of P4VP. Figure 3(b) presents room-temperature FTIR spectra in the range 970–1020 cm^{-1} for blends of OP-POSS and PS-*b*-P4VP. The P4VP block provided a characteristic band at 993 cm^{-1}, corresponding to the free pyridyl rings. Upon the blending of PS-*b*-P4VP with OP-POSS, a new band appeared at 1006 cm^{-1}, which we assign to the hydrogen-bonded pyridyl rings of the P4VP block. All of the signals for the pyridyl groups split into two bands that could be fitted well to the Gaussian function. Table 2 summarizes the results from curve fitting; the fraction of hydrogen-bonded pyridyl rings increased upon increasing the OP-POSS content in this blend system, similar to our previously reported findings for phenolic/P4VP and PVPh/P4VP blends.[52,53]

Figures 5 display SAXS profiles of OS-POSS/PS-*b*-P4VP hybrid complexes of various compositions at room temperatures. SAXS analysis revealed a lamellar micro-domain structure for pure PS-*b*-P4VP, judging from the scattering maxima at relative positions of 1:2:3:4. A couple of SAXS peaks located at positions of multiple q of 0.147 nm^{-1} indicated a lamellar phase having a long period of 42.7 nm, extracted from the first peak position ($2\pi/q$). In addition, the volume fraction of the PS phases in the lamellar structure was 48% for this diblock copolymer. The TEM image in Figure 6(a) reveals that the pure PS-*b*-P4VP diblock copolymer exhibited an alternating lamellar morphology and long-range-ordered pattern having a lamellar period of approximately 40 nm, consistent with the SAXS data in Figure 5. In the lower-q region, however, the peaks become broader and less intense for the OS-POSS/PS-*b*-P4VP hybrid system upon increasing the OS-POSS content [Figure 5], possibly because of the dispersion of the lamellar spacing or a very small grain size. Furthermore, the peaks shifted slightly to lower scatting vectors, indicating an increase in domain spacing. In the higher-q region,

RSC Advances Accepted Manuscript

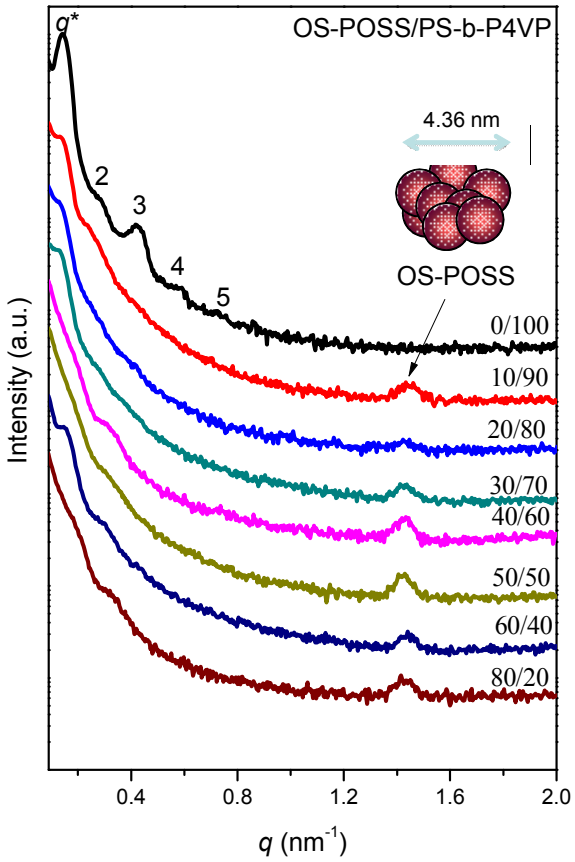

Figure 5: SAXS patterns of OS-POSS/PS-*b*-P4VP hybrids of various compositions at room temperature.

all of the blend systems provided a scattering peak at a value of 1.44 nm^{-1}, indicating a *d*-spacing of 4.36 nm that may have arisen from aggregation of the OS-POSS NPs, as depicted schematically in the inset to Figure 5,[45] because the OS-POSS NPs did not undergo the strong intermolecular interactions with the PS polymer chains that usually push such a system close to disorder at higher volume fractions of NPs. Based on the TEM images in Figure 6, the long-range order of the lamellar structure of the block copolymer PS-*b*-P4VP BCP became poor, forming distorted lamellar structures upon increasing the OS-POSS NP content up to 60 wt% [Figures 6(b)–(g)]. A further increase in the OS-POSS content to greater than 80 wt% [Figure 6(e)] led to clear macrophase separation of the OS-POSS NPs, consistent with the corresponding DSC analyses in which we observed the glass transition of pure OS-POSS.

Figure 7 displays room-temperature SAXS profiles of the OP-POSS/PS-*b*-P4VP hybrid complexes of various compositions. We observe a strong primary scattering peak (q_{max}) at all compositions, consistent with self-assembled structures exhibiting long-range order. Unlike the OS-POSS/PS-*b*-P4VP hybrid system, the SAXS profiles of these systems did not feature a scattering peak in the higher-*q* region (q = 1.44 nm^{-1}), indicating the absence of macrophase separation or aggregation of the OP-POSS NPs in the diblock copolymer PS-*b*-P4VP. In addition, we observed more well-defined, higher-order peaks, compared with those of the pure PS-*b*-P4VP, for the 10 and 20 wt% OP-POSS samples, with relative positions of 1:2:3:4:5:6:7, corresponding to lamellar structures having long-range order, as confirmed in the TEM images in Figures 8(b) and 8(c). In addition, the first-order scattering position shifted slightly to the lower-*q* region upon increasing the OP-POSS content (e.g., at 10

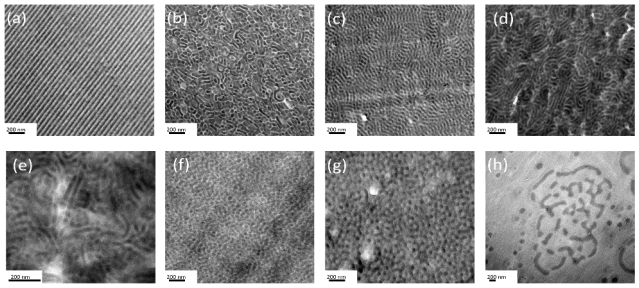

Figure 6: TEM images of OS-POSS/PS-*b*-P4VP hybrids featuring OS-POSS NP contents of (a) 0, (b) 10, (c) 20, (d) 30, (e) 40, (f) 50, (g) 60, and (h) 80 wt%.

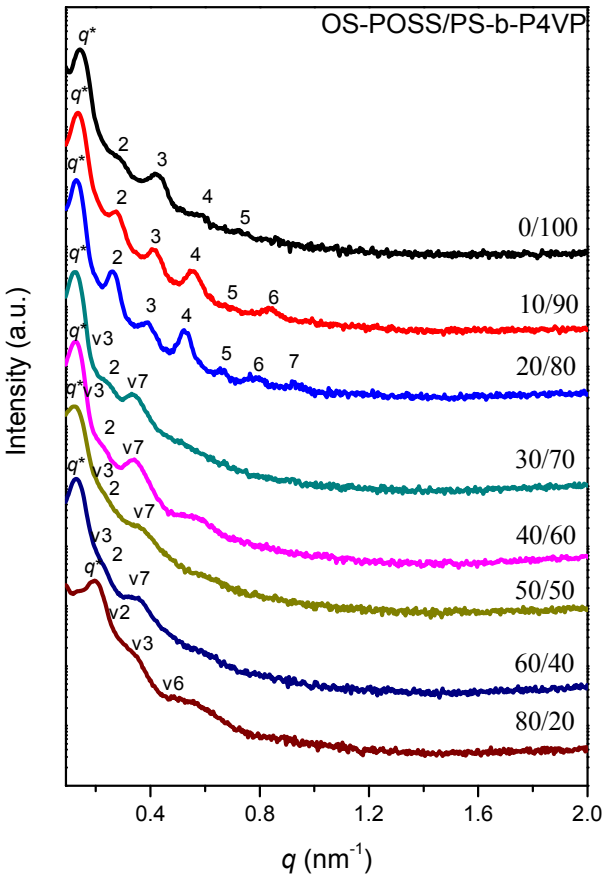

Figure 7: SAXS patterns of OP-POSS/PS-*b*-P4VP hybrids of various compositions at room temperature.

wt%: q_{max} = 0.135 nm^{-1}; *d*-spacing = 46.5 nm and at 20 wt%: q_{max} = 0.128 nm^{-1}; *d*-spacing = 49.0 nm), indicating an increase in the inter-lamellar spacing *D*. Interestingly, upon increasing the content of OP-POSS NPs to 30 wt%, a transition occurred from lamellar to cylindrical structures with a *d*-spacing of 50.1 nm. This additive-induced order–order morphological transition was driven by both increases in the effective interaction parameter and changes in the overall volume fraction between the two microphase-separated domains. Further increasing the content of OP-POSS NPs to 60 wt% did not change the peak ratios in the SAXS patterns, which revealed the 1:√3:√4:√7 ratio expected for cylindrical structures having long-range order; this behavior is confirmed in the TEM images in Figures 7, where only a slight increase in *d*-spacing, to 52.5 nm, occurred when the OP-POSS NP content reached 60 wt%. When the OP-POSS NP

RSC Advances Accepted Manuscript

This journal is © The Royal Society of Chemistry [year]

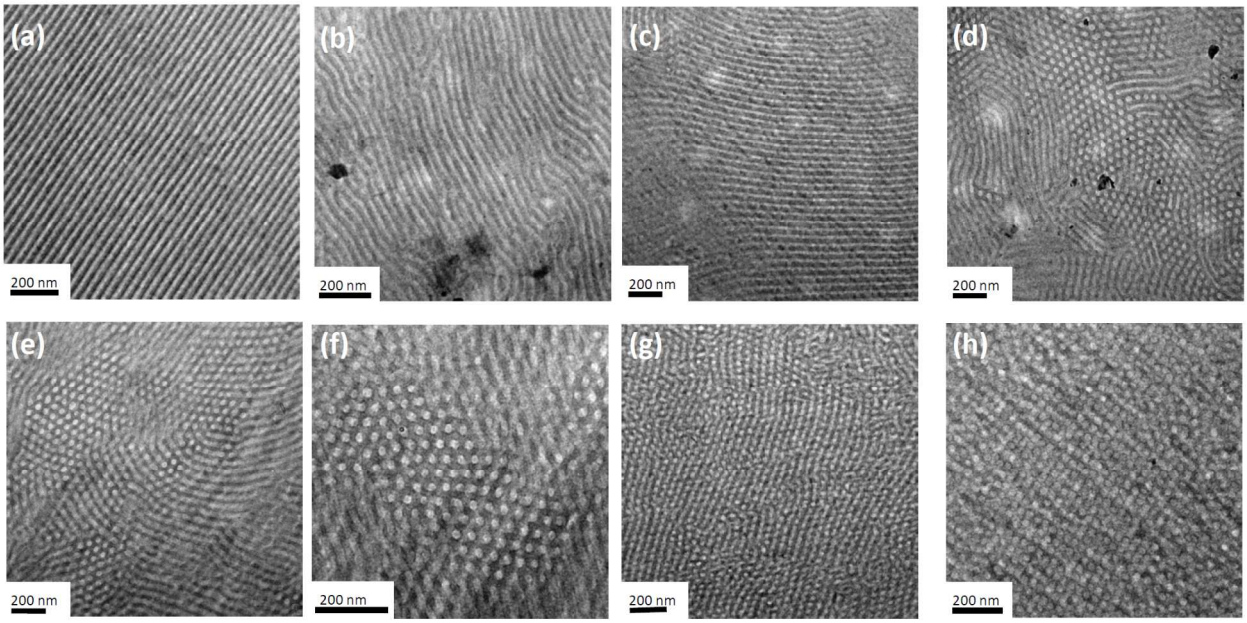

Figure 8: TEM images of OP-POSS/PS-*b*-P4VP hybrids featuring OP-POSS NP contents of (a) 0, (b) 10, (c) 20, (d) 30, (e) 40, (f) 50, (g) 60, and (e) 80 wt%.

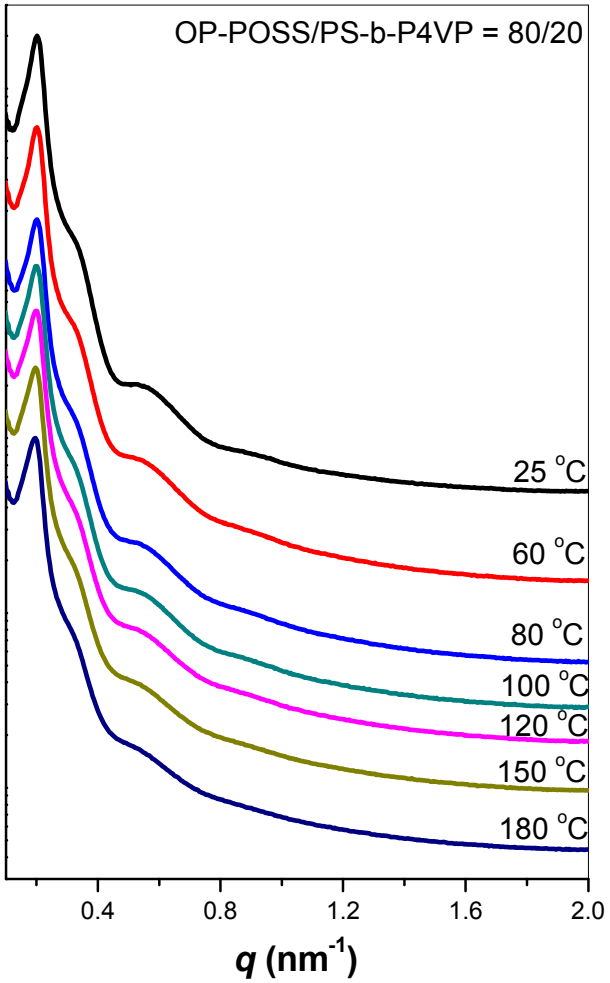

Figure 9: SAXS patterns of the OP-POSS/PS-*b*-P4VP = 80/20 hybrid at various temperatures.

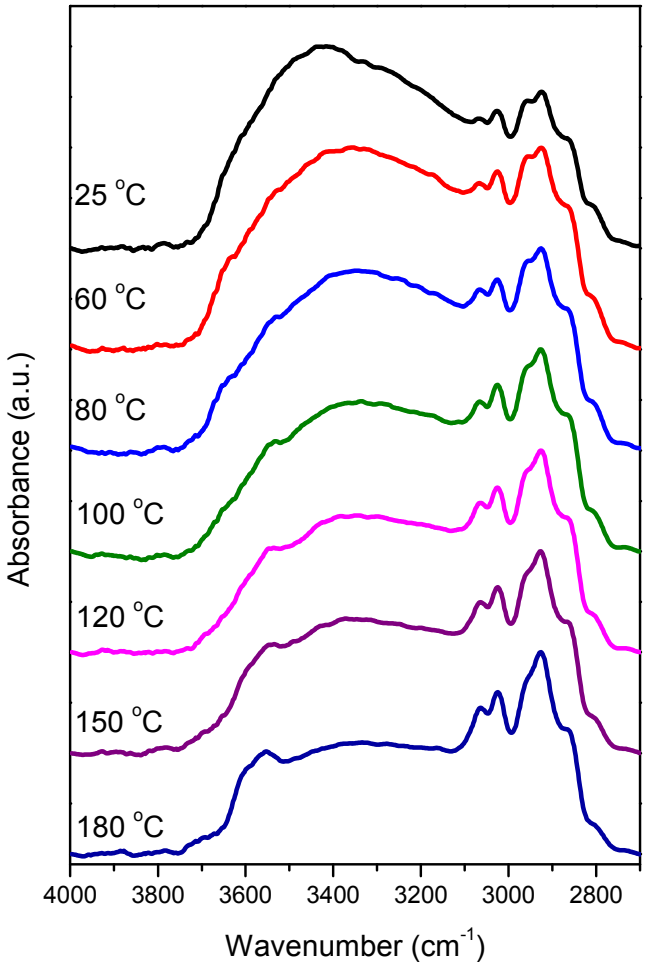

Figure 10: FTIR spectra of the OP-POSS/PS-*b*-P4VP = 80/20 hybrid at various temperatures.

RSC Advances Accepted Manuscript

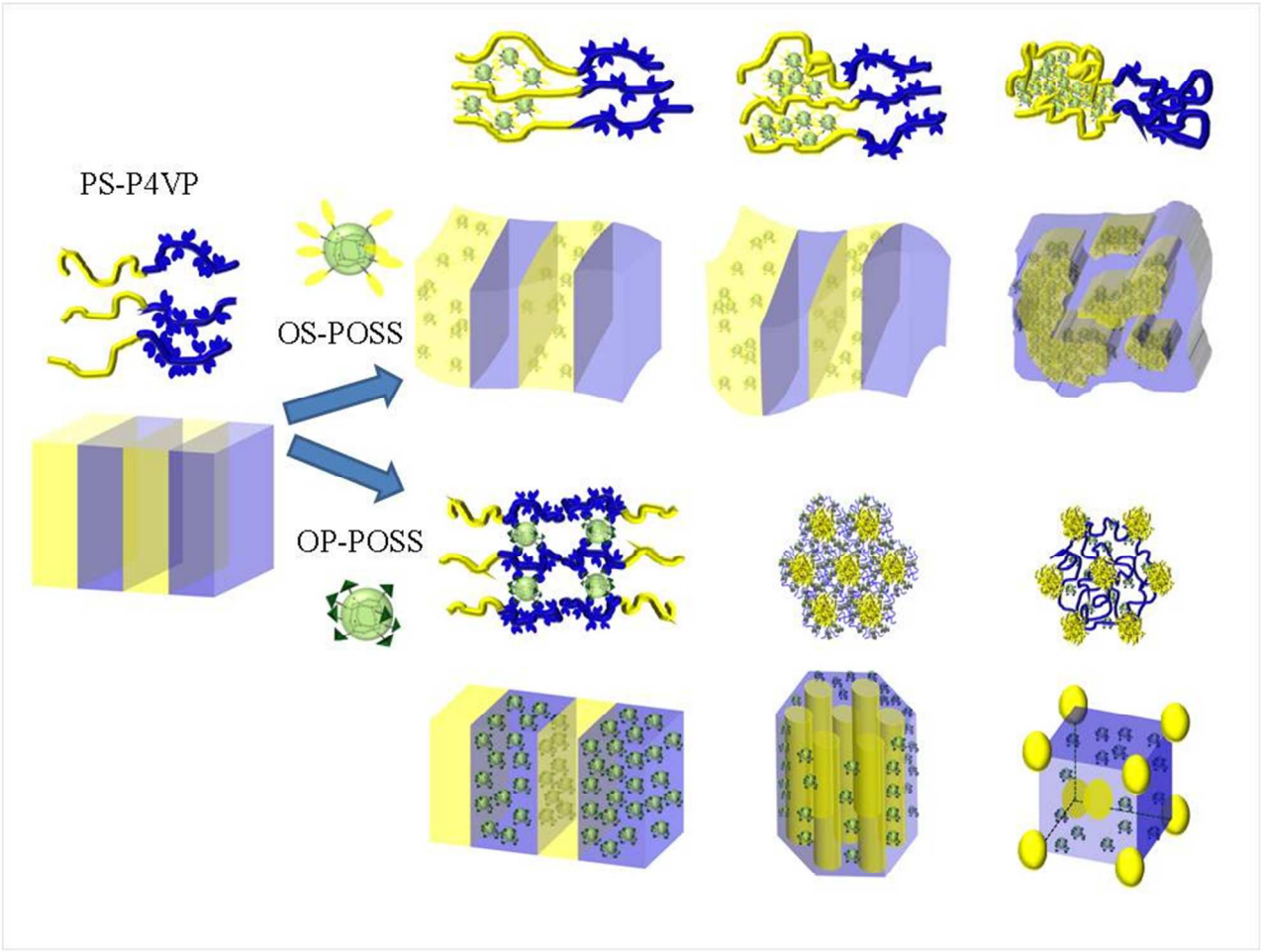

Scheme 2: Morphological changes in hybrid complexes of PS-*b*-P4VP upon increasing the content of (a) OP-POSS and (b) OS-POSS NPs.

content was 80 wt%, the SAXS pattern exhibited higher-order scattering peaks at positions in a ratio of 1:√2:√6, indicating that the morphology of this sample featured spherical micro-domains in a body-centered cubic (BCC) symmetry, consistent with the TEM images in Figure 8(h). In the TEM images in Figures 8(b)–(h), obtained without staining, we attribute the dark regions to POSS-rich layers because the Si atoms of POSS provide a high mass contrast relative to the organic domains. In the minor domain, the bright regions correspond to the PS phase and the dark regions correspond to the mixed OP-POSS/P4VP phase. The SAXS data indicate a sequence of morphological transitions that occurred upon increasing the OP-POSS content that was in good agreement with that observed using TEM: from lamellae to hexagonally packed cylinders to BCC spheres. The formation of strong hydrogen bonds between the P4VP blocks and the OP-POSS NPs was the driving force behind these morphological transitions. We were also interested in examining how the OP-POSS NPs were distributed in this hybrid. The correlated changes in the average distance a_J of the chemical junctions along the interface—and, therefore, the relative changes a_J/a_{J0} (where a_{J0} represents the value for the pure BCP)—could be derived for the complexes. Simple volumetric conservation leads to values of D/D_0 of $(\rho_J/\rho_{J0})\Phi_{block}^{-1}$ for a lamellar structure, $(\rho_J/\rho_{J0})[(2/3^{1/2})\pi(1-f)\Phi_{block}^{-1}]^{1/2}$ for a hexagonally packed cylindrical structure, and $(\rho_J/\rho_{J0})[(27\sqrt{3}/8)\pi(1-f)^2\Phi_{block}^{-1}]^{1/2}$ for BCC spheres, where D_0 is the inter-domain distance of the pure PS-*b*-P4VP (D_0 = 24.6 nm), f is the volume fraction of the PS block domain, and ρ_J is the number of block chains per unit interfacial area (ca. a_J^2); therefore, a_J/a_{J0} is approximately equal to $(\rho_J/\rho_{J0})^{-1/2}$ and Φ is the volume fraction of the BCP in the hybrid, as suggested by Hashimoto et al.[12,13] Based on these relations, we found that the values of a_J/a_{J0} for our hybrid complexes increased from 1.01 to 2.33 upon increasing the OP-POSS NP content from 10 to 80 wt%. We surmise that the added OP-POSS NPs interacted with the P4VP chains of the BCP through hydrogen bonding at their interfaces, resulting in the observed increases in the values of a_J. The PS blocks, being covalently linked to the P4VP blocks, had to contract to accommodate the expanded interfacial zone—a process that we believe led to no change in density for the BCP/NP hybrids. In addition, we suspect that the bound OP-POSS/P4VP hybrid complex simply experienced a decreased enthalpic cost at the interface. This behavior is commonly observed upon the addition of NPs—they increase the interface per chain by "hiding" the blocks from each other.

We were also interested in examining how the OP-POSS/PS-*b*-P4VP hybrid complexes behaved with respect to the temperature. Figure 9 displays SAXS profiles of OP-POSS/PS-*b*-P4VP = 80/20 recorded at different temperatures. The ratio of patterns did not change upon increasing the temperature, indicating that this hybrid complex also possessed the BCC sphere structure. Only the first-order scattering position shifted slightly, to the lower-q region, upon increasing the temperature, as a result of thermal expansion. The fraction of weaker hydrogen

RSC Advances Accepted Manuscript

This journal is © The Royal Society of Chemistry [year]

bonding interactions, such as those between OH and C=O groups, usually decreases upon increasing the temperature;[54] our FTIR spectroscopic analyses (Figure 10) revealed, however, that the strong hydrogen bonding interactions between the pyridyl units of P4VP and the OH groups of OP-POSS remained, even at 180 °C. The peak position of the signal for the OH···pyridyl interactions at 3340 cm^{-1} did not change significantly upon increasing the temperature; indeed, only the signal near 3525 cm^{-1} for the free OH groups increased accordingly. This decrease in hydrogen bonding strength did not change the self-assembled structure formed by the OP-POSS/PS-*b*-P4VP hybrid system.

Scheme 2 plots the morphological transformations of PS-*b*-P4VP that occurred upon increasing the contents of OS-POSS and OP-POSS NPs. Pure PS-*b*-P4VP exhibited the long-range order of a lamellar structure. Increasing the OS-POSS NP content up to 30 wt% disrupted the long-range order of the lamellar structures, resulting in distorted lamellae; a further increase in the OS-POSS content to greater than 80 wt% led to macrophase separation of the OS-POSS NPs. In contrast, increasing the OP-POSS NP content up to 20 wt% had no effect on the lamellar structure; further increasing the content of OP-POSS NPs to greater than 60 wt% resulted in the cylindrical structures, and 80 wt% resulted in the BCC spheres. These order–order morphological transitions—from lamellae to hexagonally packed cylinders to BCC spheres—were due to hydrogen bonding interactions between the OH groups and pyridyl units in the OP-POSS/P4VP hybrid complexes and to changes in the overall volume fractions of the two microphase-separated domains.

Conclusions

We have used DSC, TEM, SAXS, and FTIR spectroscopy to investigate, in detail, the miscibility, phase behavior, and hydrogen bonding interactions in OS-POSS/PS-*b*-P4VP and OP-POSS/PS-*b*-P4VP hybrid complexes. The structures that self-assembled from the BCP composites depended significantly on the nature of the functional groups presented by the POSS NPs. The relatively weak intermolecular aromatic hydrophobic attraction between the aromatic groups of OS-POSS and the PS block segments pushed the BCP close to disorder at higher contents of the OS-POSS NPs. The relatively strong hydrogen bonds between the OH groups of the OP-POSS NPs and the pyridyl units of the P4VP blocks induced order–order morphological transitions from lamellae to hexagonally packed cylinders to BCC spheres. No macrophase separation occurred when we blended PS-*b*-P4VP with the OP-POSS NPs, even at 80 wt%. We aim to use this information to design BCP/NP hybrids exhibiting interesting optical, electrical, and magnetic properties.

Acknowledgment

This study was supported financially by the National Science Council, Taiwan, Republic of China, under contracts NSC 100-2221-E-110-029-MY3 and NSC 100-2628-E-110-001. We thank Mr. Hsien-Tsan Lin of the Regional Instruments Center at National Sun Yat-Sen University for helping with the TEM experiments.

References

1. L. Zhu, S. Z. D. Cheng, P. Huang, Q. Ge, R. P. Quirk, E. L. Thomas, B. Lozt, B. S. Hsiao and F. Yeh, *Adv. Mater.* 2002, **14**, 31-34.
2. J. Z. Zhang, *Acc. Chem. Res.* 1997, **30**, 423-429.
3. A. C. Balazs, T. Emrick and T. P. Russell, *Science* 2006, **314**, 1107-1110.
4. J. Y. Cheng, C. A. Ross, V. Z. H. Chan, E. L. Thomas,; R. G. H. Lammertink and G. J. Vancso, *Adv. Mater.* 2001, **13**, 1174-1178.
5. T. F. Jaramillo, S. H. Baeck, B. R. Cuenya and E. W. McFarland, *J. Am. Chem. Soc.* 2003, **125**, 7148-7149.
6. B. Sarkar and P. Alexandridis, *Langmuir* 2012, **28**, 15975-15986.
7. J. J. Chiu, B. J. Kim, E. J. Kramer and D. J. Pine, *J. Am. Chem. Soc.* 2005, **127**, 5036-5037.
8. B. J. Kim, J. Bang, C. J. Hawker and E. J. Kramer, *Macromolecules* 2006, **39**, 4108-4114.
9. S. C. Park, B. J. Kim, C. J. Hawker, E. J. Kramer, J. Bang and J. S. Ha, *Macromolecules* 2007, **40**, 8119-8124.
10. J. J. Chiu, B. J. Kim, G. R. Yi, J. Bang, E. J. Kramer and D. J. Pine, *Macromolecules* 2007, **40**, 3361-3365.
11. B. J. Kim, G. H. Fredrickson and E. J. Kramer, *Macromolecules* 2008, **41**, 436-447.
12. T. Hashimoto, H. Tanaka and H. Hasegawa, *Macromolecules* 1990, **23**, 4378-4386.
13. T. Tanaka, H. Hasegawa and T. Hashimoto, *Macromolecules* 1991, **24**, 240-251.
14. H. F. Lee, S. W. Kuo, C. F. Huang, J. S. Lu, S. C. Chan, C. F. Wang and F. C. Chang, *Macromolecules* 2006, **39**, 5458-5465.
15. Y. Matsushita, *Macromolecules* 2007, **40**, 771-776.
16. N. Hameed and Q. Guo, *Macromolecules* 2008, **41**, 7596-7605.
17. K. Dobrosielska, S. Wakao, A. Takano and Y. Matsushita, *Macromolecules* 2008, **41**, 7695-7698.
18. K. Dobrosielska, S. Wakao, J. Suzuki, K. Noda, A. Takano and Y. Matsushita, *Macromolecules* 2009, **42**, 7098-7102.
19. W. C. Chen, S. W. Kuo, U. S. Jeng and F. C. Chang, *Macromolecules* 2008, **41**, 1401-1410.
20. W. C. Chen, S. W. Kuo, C. H. Lu and F. C. Chang, *Macromolecules* 2009, **42**, 3580-3590.
21. I. H. Lin, S. W. Kuo and F. C. Chang, *Polymer* 2009, **50**, 5276-5287.
22. S. C. Chen, S. W. Kuo, U. S. Jeng, C. J. Su and F. C. Chang, *Macromolecules* 2010, **43**, 1083-1092.
23. S. W. Kuo, *Polym. Inter.* 2009, **58**, 455-464.
24. V. Prysmitsyn, S. H. Han, J. K. Kim and V. Ganesan, *Macromolecules* 2012, **45**, 8729-8742.
25. U. S. Jeng, Y. S. Sun, H. J. Lee, C. H. Hsu, K. S. Liang, S. W. Yeh and K. H. Wei, *Macromolecules* 2004, **37**, 4617-4622.
26. S. W. Yeh, K. H. Wei, Y. S. Sun, U. S. Jeng and K. S. Liang, *Macromolecules* 2003, **36**, 7903-7907.
27. S. W. Yeh, K. H. Wei, Y. S. Sun, U. S. Jeng and K. S. Liang, *Macromolecules* 2005, **38**, 6559-6565.
28. C. H. Lu, S. W. Kuo, W. T. Chang and F. C. Chang, *Macromol. Rapid Commun.* 2009, **30**, 2121-2127.
29. S. W. Kuo and H. Y. Yang, *Macromol. Chem. Phys.* 2011, **212**, 2249-2259.
30. S. G. Jang, E. J. Kramer and C. J. Hawker, *J. Am. Chem. Soc.* 2011, **133**, 16986-16996.
31. Y. Lin, V. K. Daga, E. R. Anderson, S. P. Gido and J. J. Watkins, *J. Am. Chem. Soc.* 2011, **133**, 6513-6516.
32. V. K. Daga, E. R. Anderson, S. P. Gido and J. J. Watkins, *Macromolecules* 2011, **44**, 6793-6799.
33. A. Noro, K. Higuchi, Y. Sageshima and Matsushita, Y. *Macromolecules* 2012, **45**, 8013-8020.
34. S. G. Jang, A. Khan, C. J. Hawker and E. J. Kramer, *Macromolecules* 2012, **45**, 1553-1561.
35. T. Lin, R. M. Ho and J. C. Ho, *Macromolecules* 2009, **42**, 742-751.

RSC Advances Accepted Manuscript

36. (a) Y. R. Wu, Y. C. Wu and S. W. Kuo, *Macromol. Chem. Phys.* 2013, **214**, 1496-1503. (b) M. Ramanathan, S. M. Killbey, Q. Ji, J. P. Hill, and K. Ariga, *J. Mater. Chem.* 2012, **22**, 10389-10405. (c) W. Ding, J. Lin, K. Yao, J. W. Mays, M. Ramanathan, and K. Hong, *J. Mater. Chem. B* 2013, **1**, 4212-4216.
37. Y. C. Wu and S. W. Kuo, *J. Mater. Chem.* 2012, **22**, 2982-2991.
38. S. W. Kuo and F. C. Chang, *Prog. Polym. Sci.* 2011, **36**, 1649-1696.
39. H. Xu, S. W. Kuo, J. S. Lee and F. C. Chang, *Macromolecules* 2002, **35**, 8788-8793.
40. H. C. Lin, S. W. Kuo, C. F. Huang and F. C. Chang, *Macromol. Rapid Commun.* 2006, **27**, 537-541.
41. B. B. Jiang, W. Tao, X. Lu, Y. Liu, H. B. Jin, Y. Pang, X. Y. Sun, D. Y Yan and Y. F. Zhou, *Macromol. Rapid Commun.* 2012, **33**, 767-772.
42. H. Ghanbari, B. G. Cousins and A. M. Seifalian, *Macromol. Rapid Commun.* 2011, **32**, 1032-1046.
43. C. C. Cheng, Y. C. Yen and F. C. Chang, *Macromol. Rapid Commun.* 2011, **32**, 927-932.
44. (a) L. Cui, D. Y. Chen and L. Zhu, *ACS Nano* 2008, **2**, 921-927. (b) X. Zhao, W. Zhang, Y. Wu, H. Liu, and X. Hao, *New J. Chem.* 2014, **38**, 3242-3249.
45. Y. C. Sheen, C. H. Lu, C. F. Huang, S. W. Kuo and F. C. Chang, *Polymer* 2008, **49**, 4017-4024.
46. Y. J. Yen, S. W. Kuo, C. F. Huang, J. K. Chen and F. C. Chang, *J. Phys. Chem. B* 2008, **112**, 10821-10829.
47. K. W. Huang, L. W. Tsai and S. W. Kuo, *Polymer* 2009, **50**, 4876-4887.
48. S. W. Kuo, H. C. Lin, W. J. Huang, C. F. Huang and F. C. Chang, *J. Polym. Sci.: Polym. Phys.* 2006, **44**, 673-686.
49. C. H. Lu, J. H. Wang, F. C. Chang and S. W. Kuo, *Macromol. Chem. Phys.* 2010, **211**, 1339-1347.
50. C. L. Lin, W. C. Chen, C. S. Liao, Y. C. Su, C. F. Huang, S. W. Kuo and F. C. Chang, *Macromolecules* 2005, **38**, 6435-6444.
51. T. Kwei, *J. Polym. Sci., Polym. Lett. Ed.* 1984, **22**, 307-313.
52. S. W. Kuo, P. H. Tung and F. C. Chang, *Macromolecules* 2006, **39**, 9388-9395.
53. S. W. Kuo, C. L. Lin and F. C. Chang, *Polymer* 2002, **43**, 3943-3949.
54. M. M. Coleman, J. F. Graf and P. C. Painter, "Specific Interactions and the Miscibility of Polymer Blends. Technomic Publishing", Lancaster, PA, 1991.

RSC Advances Accepted Manuscript

This journal is © The Royal Society of Chemistry [year]

CREATED USING THE RSC ARTICLE TEMPLATE (VER. 3.1) - SEE WWW.RSC.ORG/ELECTRONICFILES FOR DETAILS

A Graphic Content

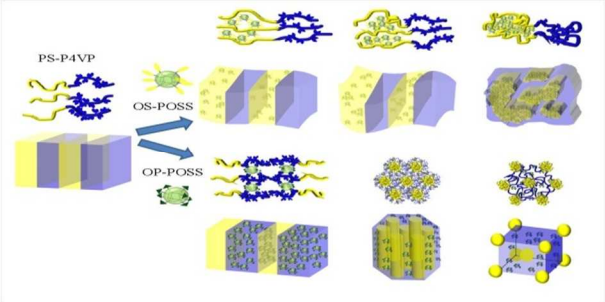

The influence of the functional groups presented by polyhedral oligomeric silsesquioxane (POSS) nanoparticles (NPs) on the self-assembled structures formed by diblock copolymer composites was detail discussed. The long-range order transformed into distorted lamellar structures when we blended PS-*b*-P4VP with the OS-POSS NPs due to the relatively weak intermolecular hydrophobic forces. In contrast, well-defined self-assembled structures, in the form of block copolymer nanocomposites, after blending PS-*b*-P4VP with the OP-POSS NPs through strong hydrogen bonding interaction.

RSC Advances Accepted Manuscript